Evaluation of the high temperature oxidation of W-Cr-Zr self-passivating alloys

X.Y. Tan[a,b*], F. Klein[b], A. Litnovsky[b], T. Wegener[b], J. Schmitz[b,d], Ch. Linsmeier[b], J.W. Coenen[b], U.Breuer[c], M. Rasinski[b], P. Li[a], L.M. Luo[a], Y.C. Wu[a*]

[a]*School of Materials Science and Engineering, Hefei University of Technology, 230009 Hefei, China;*

[b]*Forschungszentrum Jülich GmbH, Institut für Energie- und Klimaforschung – Plasmaphysik, Partner of the Trilateral Euregio Cluster (TEC), 52425 Jülich, Germany;*

[c]*Forschungszentrum Jülich GmbH, Zentralinstitut für Engineering, Elektronik und Analytik –Analytik, 52425 Jülich, Germany;*

[d]*Department of Applied Physics, Ghent University, 9000 Ghent, Belgium;*

*Corresponding author: X.Y. Tan and Y.C. Wu

Email address: jscltan2012221@163.com (X.Y. Tan), ycwu@hfut.edu.cn (Y.C. Wu)

Abstract: W-Cr-Zr systems with different compositions were oxidized in a mixed gas (Ar + 20 vol.% O_2) atmosphere at 1000 ºC. The power law which was used to describe the oxidation behaviour, indicates that W-11.2wt.%Cr-1.7wt.%Zr has an excellent oxidation behaviour. As analysed from the ten-hour exposure, W-Cr-Zr thin film oxidation shows a self-passivating stage followed by a linear oxidation stage. In addition, a study on the addition of zirconium indicates that zirconia particles act as diffusion barriers for the chromium cation diffusion and in addition function as the nucleation sites for the formation of the initial oxide scale.

Keywords: Future fusion power plant; Loss-of coolant accident; Self-passivating W alloy; W-Cr-Zr alloy; Oxidation resistance

1. Introduction

Tungsten (W) is considered as a promising candidate material for the first wall cladding in future fusion power plants, because of advantages like a high melting point, excellent thermal conductivity, high sputtering threshold and low tritium retention [1]. However, the first wall may face a safety risk in form of a loss-of-coolant accident accompanied by air ingress. This hypothetical case would lead to a temperature rise to 1000 °C after ~10 days due to the nuclear decay heat of the in-chamber components [2]. Air ingress leads to oxidation of the neutron-irradiated W and formation of volatile oxides [3]. From the current study, the oxidation behaviour of W thin film at 1000 °C is worse than linear oxidation behaviour, i.e. the oxidation rate increases with isothermal time. The volatile oxides contain a large fraction of radioactive nuclides. To prevent the sublimation of the highly radioactive oxides, high oxidation resistance self-passivating W alloys were proposed [4-6].

Self-passivating W alloys aim at forming a dense oxide scale on the surface and preventing further oxidation of W. The oxide scale forms due to preferential oxidation of passivating elements. Several requirements are imposed on the selection of a passivating element [7]:

- low radioactivity[1],
- high melting point,
- suitable Pilling-Bedworth ratio[2],
- good adhesion to the matrix.

[1] Short half-life time of the neutron irradiated material.

[2] PBR is the ratio of the volume of the oxide to that of pure metal [8], we use it as a merit of the volume increase during oxidation.

Chromium (Cr) as a passivating element has been extensively applied in antioxidant steels [9-11] and self-passivating W alloys [3-7]. In the W-Cr binary alloys [3,12], voids were detected at the interface between oxide scale and matrix. In case of continuous oxidation, the Cr_2O_3 scale would crack and even spall, which will result in W oxidation. A small amount of an active element was proposed to improve this behaviour. The major effects of the active element are improvement in the scale adherence and strengthening of the oxide scale [13]. According to the current understanding, an active element should have higher oxygen affinity and lower PBR relative to the passivating element. Yttrium (Y) is widely known as an active element, extensively applied in Fe-Cr alloys [14,15]. In recent studies [12,16], Y has also been added as an active element in self-passivating W alloys and shows an excellent oxidation resistance.

In the present work, Zirconium (Zr) as an active element was proposed to improve the oxidation behaviour of the self-passivating W-based alloy especially with respect to long-term oxidation. Zr has good oxygen affinity [17], acceptable radioactivity [18], low PBR and a high melting point (~1855 ºC). In order to optimize the composition, a series of W-Cr-Zr thin film samples with different compositions has been produced by magnetron sputtering technique. Oxidation tests were conducted to evaluate the corresponding oxidation behaviour. In addition, detailed studies on the influence of Zr as an active element on the behaviour of Cr during the oxidation process were carried out.

2. Materials and methods

2.1 Preparation of samples

In this work, all of the studied samples are thin film samples, which are produced using a magnetron sputtering technique (PREVAC, Poland). Sputter targets of W, Cr and Zr with the same purity of 99.95 wt. % were supplied by the Kurt J. Lesker Company and the MaTeck GmbH. The W target and Cr target were mounted to the DC-magnetron whereas the Zr target was biased though RF-mode power. These metal elements were deposited on sapphire substrates of a diameter of 12 mm. The magnetron sputtering procedure was conducted under high vacuum conditions with a residual pressure lower than 1×10^{-5} mbar, which was necessary for avoiding oxygen. For the W-Cr-Zr system, the series of W-Cr-Zr samples were produced with the same deposition time of 90 min. In order to obtain a homogeneous structure, all targets were sputtered at the same time and the sample holder was kept at a rotation speed of 20 º/s. W-Cr-Zr samples with different compositions were obtained by adjusting the power of the corresponding magnetron targets. To investigate how Zr influences the behaviour of Cr during the oxidation process, two kinds of thin film samples with a double-layered structure were designed. Firstly, a pure Cr layer with a thickness of ~ 2.2 μm was sputtered on the sapphire substrates, then one sample was deposited with a pure Zr layer and another sample was deposited with Cr-Zr composite layer. Here, these two kinds of double-layered thin film samples are denoted by Cr-Zr and Cr-Cr/Zr, respectively. In addition, a pure Cr thin film sample was produced for reference.

2.2 Oxidation experiments

The oxidation behaviour was investigated using a thermal gravimetric analysis (TGA) facility (TGA 16 from SETARAM) in a gas mixture of 80 vol.% Ar and 20 vol.% O_2 with a pressure of 1 bar at 1000 °C. The purity of the Ar or O_2 was 99.9999%. The flow rate of the mixture gas was 20 ml/min during the oxidation process. The TGA facility can measure in-situ weight change during the high temperature oxidation process as a function of time. The TGA facility was equipped with a double symmetrical furnace: one of the two furnaces was used for the produced sample oxidation tests; the other furnace was used for correction measurements. Therefore, considering the influence of buoyancy, gas velocity and temperature, correction measurements have been carried out with pure sapphire substrate, simultaneously. Firstly, for each of the series of investigations of W-Cr-Zr samples, an isothermal oxidation was conducted for 75 min. According to the oxidation curves, the most promising candidate alloy compositions were selected for longer oxidation tests for 10 h at 1000 °C to clarify the corresponding

oxidation behaviour. Furthermore, the oxidation experiments with pure Cr, Cr-Zr and Cr-Cr/Zr thin film samples were carried out in the same oxidation atmosphere with an isothermal time of 1 h.

Fig. 1 presents the temperature and Ar flow rate profiles of the oxidation process with an isothermal oxidation for 75 min. Each of these studied samples was hanged into a triangle holder and heated with the furnace. To avoid sample oxidation during the heating stage, the furnace chamber was conditioned by a vacuum pumping process before heating. At the heating stage, the heating rate was 20 °C/min. When the temperature reached 150 °C, the TGA system was proceed by vacuum pumping again to further decrease the level of residual oxygen. Considering gas flow rate would effect on the weight change, the Ar flow rate was changed from 100 ml/min to 20 ml/min when the temperature reached 560 °C. At the holding stage, the sample underwent the isothermal oxidation test in a gas mixture of Ar and 20 vol.% O_2 at a flow rate of 20 ml/min. The weight change during oxidation was recorded at a frequency of 1 Hz. For the cooling stage, the furnace was cooled at a cooling rate of 40 °C/min in Ar atmosphere. These details are depicted in Fig. 1. For the longer oxidation of the optimized W-Cr-Zr samples and the double-layered samples of Cr-Zr and Cr-Cr/Zr, the heating and cooling stage of the oxidation process are the same as shown in Fig. 1. The holding time is varied for different experiments.

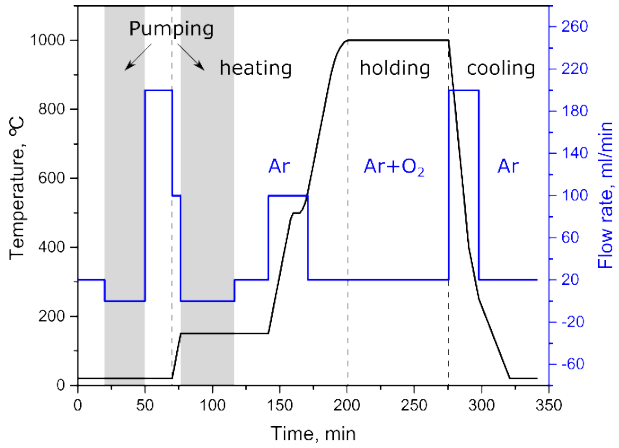

Fig. 1 Temperature and gas flow rate profiles of the oxidation process.

2.3 Characterization

For each composition of the W-Cr-Zr system, one sample was selected for inductively coupled plasma optical emission spectrometry (ICP-OES) to measure the corresponding composition. The W-Cr-Zr sample was completely dissolved with a mixture of 3 mL H_3PO_4 and 3mL $HClO_4$ in Berghof pressure digestion at 200 ºC. After duration of 6 hours, the digested solution was diluted and then used for analysis. Table 1 shows the compositions of these W-Cr-Zr samples by weight percent (wt.%) and atomic percent (at.%) from the ICP-OES technique. Traditionally, W-Cr-Zr samples are named after their composition in wt.%. However, the high temperature oxidation of metals or alloys can be considered as a cation diffusion process [19-22], which is relate to the concentration of the diffusion atoms. Thus, it is worth to compare the composition of these W-Cr-Zr samples from the perspective of atomic percent. From Table 1, there exist two series of W-Cr-Zr samples with a similar Cr content of ~28.96 at.% and ~30.44 at.%, respectively. One series is W-10.4Cr-0.8Zr, W-10.5Cr-1.3Zr and W-10.5Cr-1.9Zr; and the other series is W-11.2Cr-1.7Zr, W-11.2Cr-3.6Zr and W-12.5Cr-7.0Zr. In addition, W-9.6Cr-1.9Zr and W-10.5Cr-1.9Zr have a similar Zr content of ~3.05 at.%; W-10.4Cr-0.8Zr and W-12.5Cr-0.6Zr also have a similar Zr content. Comparison of the change laws between the properties and composition of W-Cr-Zr samples is done using units of atomic percent in this work.

Table 1. The composition of the obtained W-Cr-Zr thin film samples

Thin film samples	Composition					
	W		Cr		Zr	
	wt.%	at. %	wt.%	at. %	wt.%	at. %
W-9.6Cr-1.9Zr	88.46	69.95	9.63	26.93	1.91	3.12
W-10.4Cr-0.8Zr	88.79	69.78	10.41	28.92	0.80	1.30
W-10.5Cr-1.3Zr	88.19	68.87	10.52	29.05	1.29	2.08
W-10.5Cr-1.9Zr	87.62	68.10	10.52	28.91	1.86	2.99
W-11.2Cr-1.7Zr	87.12	66.91	11.21	30.44	1.67	2.65
W-11.2Cr-3.6Zr	85.18	64.39	11.22	29.98	3.60	5.63
W-12.1Cr-7.0Zr	80.90	58.58	12.07	30.90	7.03	10.52
W-12.5Cr-0.6Zr	86.91	65.68	12.49	33.38	0.60	0.94

X-ray diffraction (XRD, D8 Discover, Bruker) was used to evaluate the phase structure of the samples as deposited and after oxidation. Scanning electron microscopy (SEM, Carl Zeiss Crossbeam 540) equipped with focused ion beam (FIB) was also used to characterize the surface morphology or cross section of some representative W-Cr-Zr samples before and after oxidation. For FIB cutting, the sample surface was deposited with a platinum (Pt) layer, which protects the surface from damages during cutting. In addition, to figure out the influence of Zr in the oxidation process, the Cr-Zr or Cr-Cr/Zr samples were analysed by SEM-FIB and the time-of-flight secondary ion mass spectrometry (TOF-SIMS, fourth generation, ION-TOF GmbH) analyser in the dual beam mode. The TOF-SIMS analyser aims at investigating the elements depth profile of the Cr-Zr and Cr-Cr/Zr samples. In this SIMS measurement, the sputtering oxygen ions beam (O_2^+) with energy of 2 keV was applied on an area of 300 μm × 300 μm for sputtering a crater. The measurement bismuth ions beam (Bi^+, Bi^{3+}) with energy of 25 keV was progressively analysing the crater bottom in an area of 51 μm × 51 μm.

2.4 Evaluation of the oxidation behaviour

Evaluation of the oxidation behaviour was based on the analysis of the oxide scale growth. Several growth laws have been applied to describe the oxidation behaviour such as linear, logarithmic, parabolic and cubic laws. The linear law was based on the surface reaction step towards the reactive gases of the environment [19], which is used to describe the oxidation of non-passivating materials. The growth rate is independent of the time of the oxidation. The other growth laws are applied to evaluate the oxidation behaviour of the passivating materials. The logarithmic law was used to evaluate the growth behaviour of very thin oxide film in the range of 2-10 nm during the initial few minutes [20]. For the parabolic or cubic law, the growth rates are inversely proportional to thickness and squared thickness of the scale, respectively. According to the responding theories and analyses in [19-22], the growth laws of the passivating materials are correlated with ion diffusion. Among these oxide scale growth laws, the parabolic law is the most commonly used law that has been in-depth studied. The parabolic law [23] was first demonstrated experimentally by Tammann [24]. Based on the mechanism of the parabolic law from the Wagner's oxidation theory [21], the oxidation process of the passivating material is determined by ion diffusion. The thickness of the oxide scale is proportional to the ion diffusion depth of oxidation. Therefore, the scale growth rate can be written as $\frac{dX(t)}{dt} = \frac{k_p}{X(t)}$ [25], where $X(t)$ is the thickness of the oxide scale over oxidation time (t) and k_p is the oxidation rate constant of the parabolic oxidation.

Since the mass change per unit area ($\Delta m/A$) is equivalent to the thickness of the oxide scale, the relationship between $\Delta m/A$ and time (t) obeys the parabolic law [3-8]. The mass change can be in-situ measured with the TGA facility and the area (A) of the tested samples can also be measured. The corresponding expression of the parabolic law can be written as

$$\left(\frac{\Delta m}{A}\right)^2 \propto k_p \cdot t \quad (1).$$

Nevertheless, Wagner's oxidation theory is based on several assumed conditions [26]: Wagner's theory requires that the oxidation product should be a dense, homogeneous, and relatively thick layer of oxide; formation of one oxide; and chemical equilibrium at each interface between different phases. These requirements are hard to satisfy at the same time in polycrystalline material [27,28]. Therefore, the parabolic law fails to exactly describe the oxidation behaviour of the passivating material, because the ion diffusion rate is not exactly proportional to $1/X(t)$. Based on the current understanding of the oxidation kinetics, we suppose that the oxide scale growth rate should be $\frac{dX(t)}{dt} = \frac{k}{X(t)^l}$, where l is a dimensionless impact factor that describes the relationship between ion diffusion rate and oxide scale thickness. Using the term $\Delta m/A$, the oxidation behaviour can be described by the expression (2) as below:

$$\left(\frac{\Delta m}{A}\right)^{l+1} \propto (l+1) \cdot k \cdot t \quad (2).$$

The expression (2) can also be rewritten in the form of a power law as

$$\frac{\Delta m}{A} \propto K \cdot t^n \quad (3),$$

where Δm is the mass change, A is the surface area of the sample, and t is the oxidation time, K and n are defined as the oxidation coefficient and dimensionless oxidation exponent, respectively. According to the expression (3), if $n = 1$, the power law complies with the linear oxidation behaviour; if $n = 1/2$, the power law conform to the parabolic oxidation behaviour; when $n = 1/3$, the power law follows the cubic oxidation behaviour. Therefore, the power law is a general mathematical expression to describe the oxidation performance. Furthermore, the oxidation rate (oxide scale growth rate) can be defined as the mass change per unit area per unit time (the unit is $mg \cdot cm^{-2} \cdot s^{-1}$), and the expression can be written as,

$$\frac{d}{dt}\left(\frac{\Delta m}{A}\right) \propto K \cdot n \cdot t^{n-1} \quad (4).$$

From the expression (4), when $0 < n < 1$, the oxidation rate decreases over time. The corresponding material can then be called a self-passivating material. While $n = 1$ or $n > 1$, the oxidation rate is a constant or increases over time, thus the corresponding material can be classified as a non-passivating material. Essentially, oxidation protection involves the formation of an initial thin passivating scale all over the top surface and then its continuous growth [13]. According to the current study, the oxidation coefficient (K) associated with the mass change would be required to form the full coverage of passivating scale on the top surface and the oxidation exponent (n) is closely related to the continuous growth rate of the oxide scale.

3. Results

3.1 W-Cr-Zr thin film samples

The phase structure of produced W-Cr-Zr samples as deposited was examined by XRD. Considering the composition of these W-Cr-Zr samples, the corresponding XRD spectra are shown in Fig. 2a and 2b, respectively. From Fig. 2, each of the W-Cr-Zr samples only shows a single-phase structure with body-centred cubic (bcc) structure. This finding means that the W-Cr-Zr samples have turned to a completely solid solution structure after magnetron sputtering and indirectly verifies that W-Cr-Zr samples have a homogenous microstructure. The dotted lines in Fig. 2 outline the corresponding peaks of a bcc structure. From the three peaks with the highest intensity peaks of (110), (200) and (211) in bcc structure, the W-Cr-Zr samples have the same weak orientation of (200). In other words, the deposited W-Cr-Zr samples have preferred orientation during the magnetron sputtering process. Furthermore, these peaks in Fig. 2 exhibit positional deviation in different degree, especially for the high-angle peak of (211), indicating that the deposited W-Cr-Zr samples have a different lattice constant, which is due to the different composition.

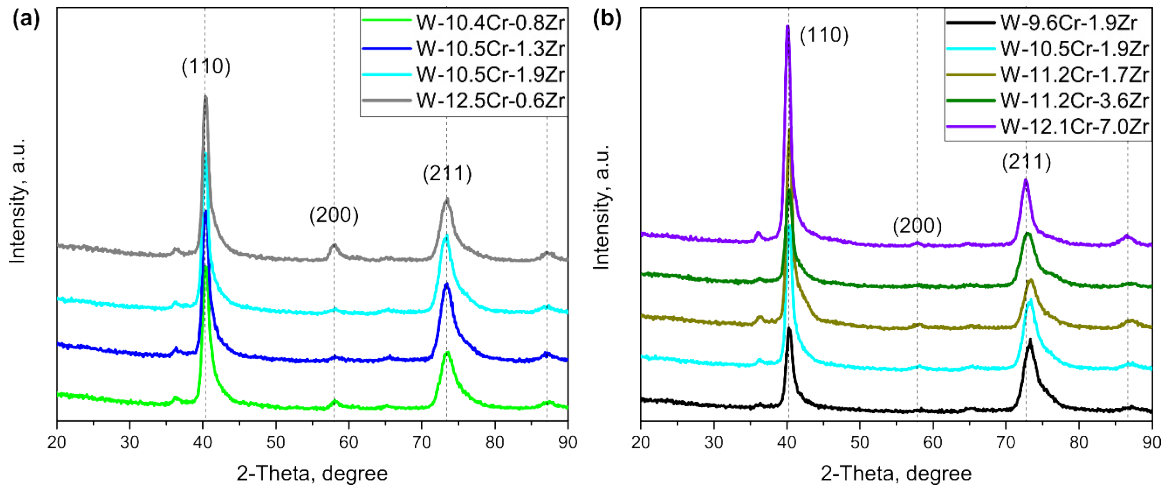

Fig. 2 XRD spectra of these W-Cr-Zr samples as deposited.

One representative sample, W-11.2Cr-1.7Zr sample, was selected to characterize the corresponding surface morphology and cross section via SEM-FIB. Fig. 3a is the surface morphology of the W-11.2Cr-1.7Zr sample, showing a uniformly distributed flake structures. The cross section of the sample is shown in Fig. 3b, finding that the thickness of the sample is approximately 4 μm. Owing to the peaks widening in the XRD spectrum (Fig. 2), the sample should possess nanoscale grains. The different grains of the sample could be distinguished by the different contrast in Fig. 3b. Notably, there is no obvious singular microstructure as observed in Fig. 3, meaning that the W-Cr-Zr sample has a homogenous microstructure.

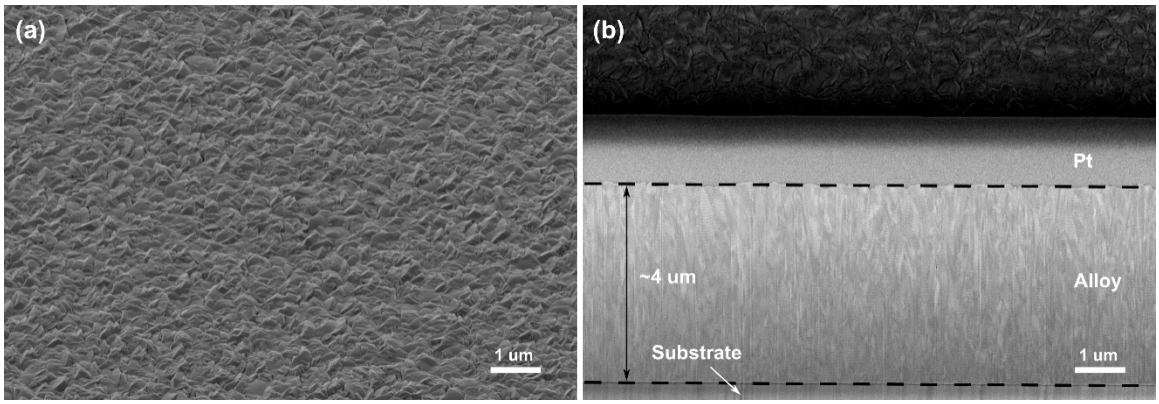

Fig. 3 (a) The surface morphology and (b) cross section of the W-11.2Cr-1.7Zr alloy as deposited

3.2 Oxidation behaviour

Each composition series of the deposited W-Cr-Zr samples underwent identical isothermal oxidation for 75 min. The corresponding oxidation curves are shown in Fig. 4a and 4b. Fig. 4a presents the oxidation curves of the W-12.5Cr-0.6Zr sample and W-Cr-Zr samples with a similar Cr content of ~28.96 at.%. Fig. 4b presents the oxidation curves of the other series of W-Cr-Zr samples with similar Cr content and the rest of the W-Cr-Zr samples. From Fig. 4, the W-10.5Cr-1.3Zr sample shows the lowest mass change, while the W-12.1Cr-7.0Zr sample exerts the highest mass change after 75 min isothermal oxidation. Notably, the oxidation rate of the W-12.5Cr-0.6Zr sample has an anomalous change after oxidation of ~ 40 min. It is hard to clearly describe the oxidation behaviour of these W-Cr-Zr samples and find out the change laws between the corresponding oxidation behaviour and composition. To evaluate the corresponding oxidation behaviour, the power law expression (3) was applied to fit these oxidation curves. The corresponding fitting curves are marked red with dotted lines as shown in Fig. 4. All fitting

curves are fitted from the start to the maximum valid time. The maximum valid time gets from the maximum applicable range of the corresponding fitting curve, which depends on the coincidence of the fitting curve and the original oxidation curve. The maximum valid time was defined as the passivating time of the W-Cr-Zr sample, which is the duration time of the self-passivating behaviour. These fitting curves as shown in Fig.4 coincide very well with the original oxidation curve in the range of the passivating time, which verifies that the power law of expression (3) is suitable to describe the oxidation behaviour of the W-Cr-Zr self-passivating alloys.

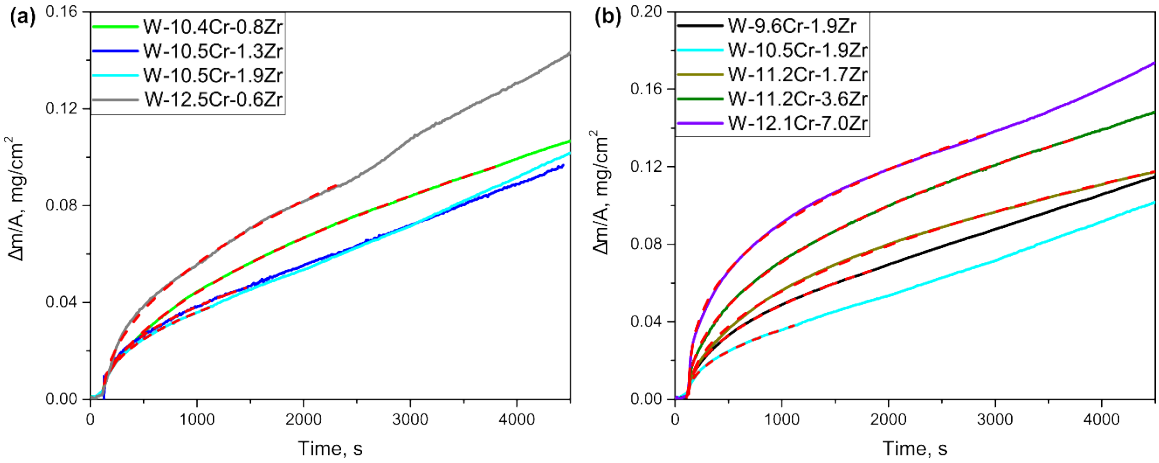

Fig. 4 The oxidation curves of the obtained W-Cr-Zr samples at 1000 ºC. Solid colour lines are the original oxidation curves and the red dotted lines are the corresponding fitting curves.

Based on the power law fitting function, the two parameters oxidation coefficient (K) and oxidation exponent (n) of these oxidized W-Cr-Zr samples can be obtained and are presented in Table 2. The parameter of the abovementioned passivating time (T) is also shown in Table 2. When combining Fig. 4 and Table 2, we found that the shape of the oxidation curve relates to the K and n in the range of the passivating time. The oxidation protection involves the formation of an initial thin passivating scale all over the top surface and then its continuous growth [13]. Therefore, we proposed that the K is associated with the mass change for forming the initial oxide scale. Further, the n is closely related to the continuous growth rate of the oxide scale. Large K value means intensive mass change at the first few moments. Low n value means moderate mass change, i.e. a low growth rate of the oxide scale at the following oxidation stage. From Table 2, Zr content affected not only the K but also the n. While the Cr content is kept constant, the K presents a change trend that increases with increasing Zr content but the n decreases with increasing Zr content. The W-12.5Cr-7.0Zr sample with the highest Zr content has the lowest n value, implying that Zr addition can reduce the growth rate of the formed oxide scale. In addition, the W-12.5Cr-7.0Zr sample also has the highest K value, indicating it requires a high mass change to form the initial thin passivating scale. For the self-passivating materials, the loss of protection arises mostly from scale cracking or spalling. The loss of protection can be reflected in the parameter of passivating time. Therefore, passivating time would be a criterion to evaluate the level of self-passivating behaviour of these studied materials. It was found that the passivating time shows the same change law with oxidation exponent when the Cr content is similar. Most notably, the W-11.2Cr-1.7Zr sample has the longest passivating time and it shows the self-passivating behaviour at the full-scale oxidation time of 75 min.

Table 2 The oxidation coefficient (K), oxidation exponent (n) and passivating time (T) of the W-Cr-Zr samples (the standard error of K and n are below 5×10^{-5} and 5×10^{-4}, respectively).

Thin film samples	*K*	*n*	*T, min*
W-9.6Cr-1.9Zr	0.00205	0.46674	30
W-10.4Cr-0.8Zr	0.00107	0.54748	61
W-10.5Cr-1.3Zr	0.00185	0.44621	31
W-10.5Cr-1.9Zr	0.00182	0.43953	17
W-11.2Cr-1.7Zr	0.00242	0.46319	75
W-11.2Cr-3.6Zr	0.00334	0.45080	61
W-12.1Cr-7.0Zr	0.00809	0.35645	47
W-12.5Cr-0.6Zr	0.00222	0.47857	37

3.3 Microstructure characterization

After isothermal oxidation of 75 min, the oxidation products of W-Cr-Zr samples were examined by XRD. Fig. 5 presents the corresponding XRD spectra, which shows that the formed oxide scale is composed of Cr_2O_3 (JCPDS # 85-0730) and ZrO_2 (JCPDS # 49-1642). There are no obvious tungsten oxide peaks in XRD spectra at least at the detection limit, indicating that the W-Cr-Zr alloy succeeds as a self-passivating material. Notably, these oxides of $CrWO_4$ (JCPDS # 70-2371) and WO_3 (JCPDS # 83-0949) can be observed in W-12.5Cr-0.6Zr sample, meaning that W has been oxidized during the 75 min oxidation test. This is mainly attributed to the too low Zr/Cr ratio limiting the protection of W oxidation, which will be explained later. In addition, the ZrO_2 peaks are very weak and only one characteristic peak can be detected because of the low content of Zr addition. Most notably, the solid solution peaks of the W-Cr-Zr samples are also observed in Fig. 5 as denoted by the dotted lines. Compared to Fig. 2, these three highest intensity peaks of (110), (200) and (211) obviously sharpen, which means that the matrix of these W-Cr-Zr samples exhibits a good crystallization property. Furthermore, the peak positions slightly deviate from the original positions in Fig. 2, i.e., the corresponding lattice constants have changed, implying that the composition of the matrix of these W-Cr-Zr samples has changed. This is may be due to the Cr and Zr depletion and formation of mixed oxides during the oxidation process.

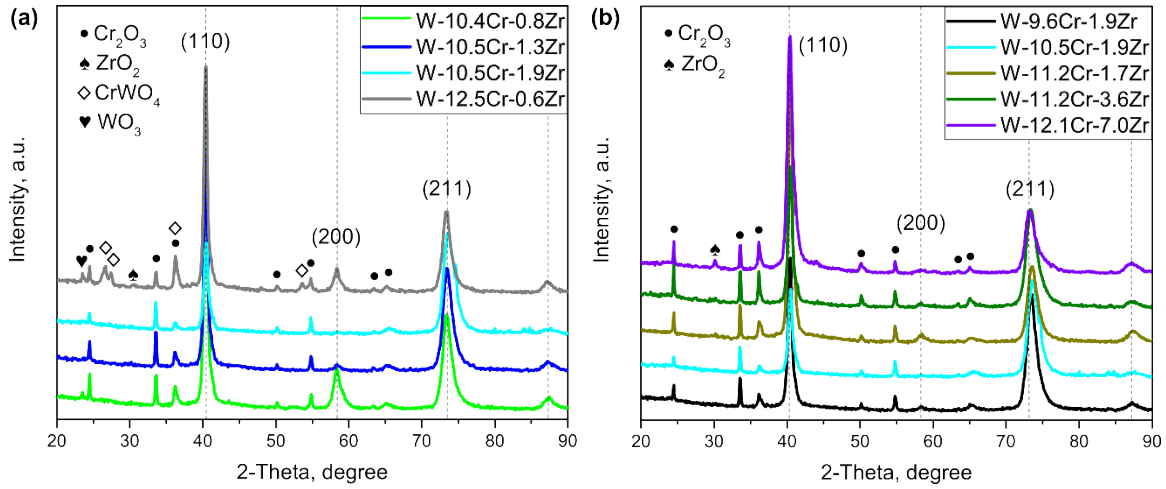

Fig. 5 *The XRD spectra of the W-Cr-Zr samples after isothermal oxidation of 75min.*

The cross sections of several representative W-Cr-Zr samples were characterized and are shown in Fig. 6. The white layers on the top surface are the deposited Pt layer. Below the Pt layer, the dark layers marked with white dotted lines represent the formed oxide scale, which is composed of Cr_2O_3 and ZrO_2 from the XRD spectra (Fig. 5). The formed oxide scale on the surface of W-Cr-Zr sample indicates that

the produced W-Cr-Zr samples exert self-passivating behaviour. The thicknesses of the corresponding oxide scales are also denoted. Notably, some punctate, linear or regional dark areas could be found in the cross section, which have a similar contrast with the surface oxide scale, thus these areas are mainly oxides formed by internal oxidation. Fig. 6a presents the cross section of the W-12.5Cr-0.6Zr sample, the thickness of the oxide sale is only ~ 230 nm. However, the W-12.5Cr-0.6Zr sample displays severe internal oxidation, which is visible almost throughout the entire thin film. The severe internal oxidation is the main reason why the W-12.5Cr-0.6Zr sample presents an anomalously changed oxidation rate in Fig. 4a. Fig. 6b and 6c are the cross sections of W-10.5Cr-1.3Zr and W-11.2Cr-1.7Zr samples, respectively. The W-10.5Cr-1.3Zr sample shows the lowest mass change in Fig. 4a, but possesses a thick oxide scale from Fig. 6b. Therefore, the lowest mass change is reflected in the small amount of internal oxidation. W-11.2Cr-1.7Zr sample with the longest passivating time possesses an oxide scale with thickness of ~ 310 nm, but possesses internal oxidation close to the surface. Remarkably, W-12.1Cr-7.0Zr sample with the highest mass change has the thickest oxide scale as shown in Fig. 6d. Furthermore, the W-12.1Cr-7.0Zr sample also exhibits severe internal oxidation that massive punctate oxides cover the entire cross section.

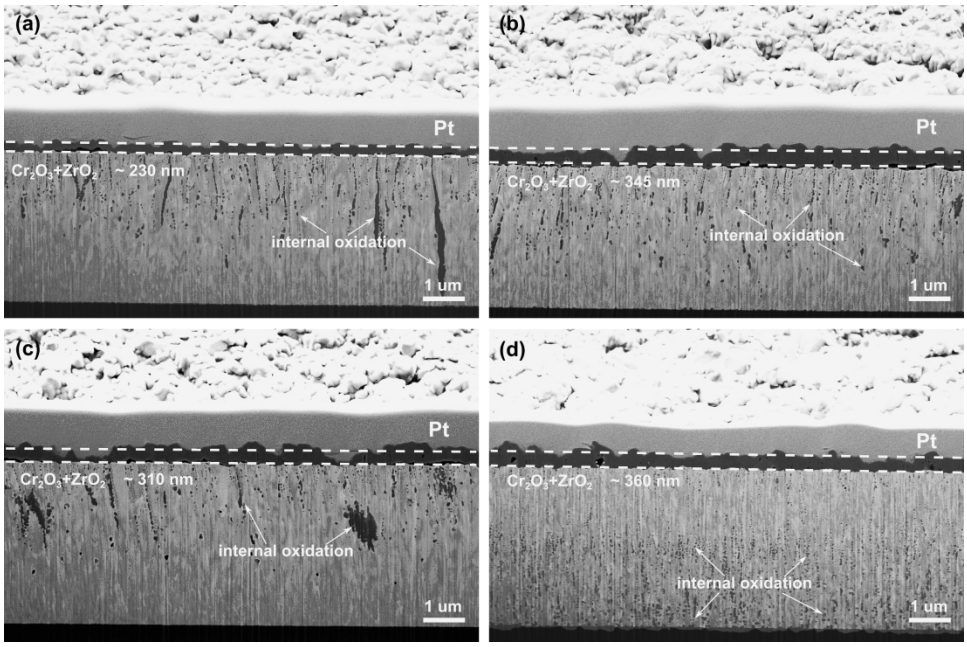

Fig. 6 The cross-section of (a) W-12.5Cr-0.6Zr, (b) W-10.5Cr-1.3Zr, (c) W-11.2Cr-1.7Zr and (d) W-12.1Cr-7.0Zr samples after isothermal oxidation of 75 min.

3.4 W-Cr-Zr optimisation

The W-11.2Cr-1.7Zr sample with the longest passivating time was used for comparison with the other thin film samples [12]. These samples are oxidized at the same conditions and the corresponding oxidation curves are shown in Fig. 7a. All oxidation curves are fitted by the power law of the expression (3) and the oxidation behaviour parameters are also shown in Fig. 7a. The pure W sample with the highest oxidation exponent of ~1.56 means sudden oxidation at the initial few minutes. The oxidation exponent value is larger than 1, indicating that the pure W oxidation behaviour is worse than linear oxidation behaviour. The W-Cr sample shows better oxidation behaviour than the pure W, but only has ~5 min passivating time. Notably, the W-Cr-Y and the W-Cr-Zr samples show similar oxidation behaviour in the tested oxidation time which have similar oxidation coefficient and oxidation exponent. In contrast to the W-Cr sample, the oxidation exponent has obviously reduced and the passivating time has significantly increased. Therefore, the Y or Zr active element additions have significantly improved the high-temperature oxidation behaviour by reducing oxidation exponent and prolonging the passivating time.

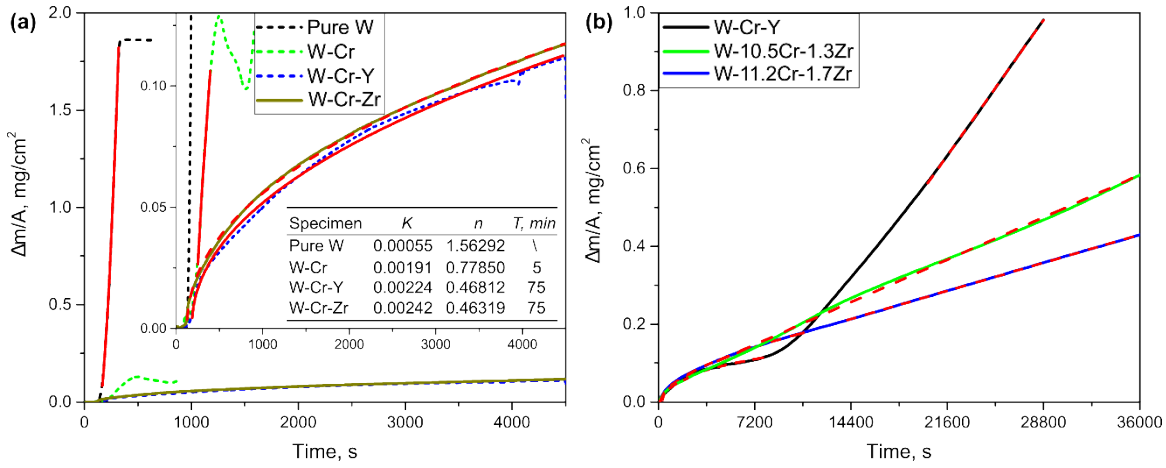

Fig. 7 (a) The oxidation behaviours of the optimal W-Cr-Zr and the referred [12] (pure W, W-Cr and W-Cr-Y) samples at 1000 ºC and duration of 75 min. (b) The longer oxidation test of W-Cr-Zr and W-Cr-Y samples. The red lines are the corresponding fitting curves.

Furthermore, the W-10.5Cr-1.3Zr sample has the lowest mass change after 75 min oxidation as can be seen in Fig. 4a. Thus the W-10.5Cr-1.3Zr and W-11.2Cr-1.7Zr samples are selected for a longer oxidation time of 10 h at 1000 ºC. Fig. 7b shows the corresponding oxidation curves and the comparison curve of the W-Cr-Y sample. The dotted lines are the corresponding fitting curves. From Fig. 7b, the longer oxidation process would contain a self-passivating stage and a linear stage. W-11.2Cr-1.7Zr has the lowest mass change after 10 h oxidation. The oxidation curves at the self-passivating stage agree with the power law, while at the linear stage they are following the linear law. The passivating times of W-Cr-Y and W-11.2Cr-1.7Zr samples are approximately 2 h and 3 h, respectively. During the linear stage, the oxidation rates of W-Cr-Y, W-10.5Cr-1.3Zr and W-11.2Cr-1.7Zr samples are 4.84×10^{-5}, 1.52×10^{-5} and 1.00×10^{-5} mg/(cm^2·s), respectively. Therefore, Zr addition could obviously reduce oxidation at the linear stage. The influence of Zr addition will be discussed later. More remarkably, the W-Cr-Y sample has a significant inflection point from the self-passivating to the linear stage, while the W-Cr-Zr samples have a smooth transition between those two stages. This finding indicates that the W-Cr-Zr sample has a low oxidation rate after the self-passivating stage. Therefore, these W-Cr-Zr samples show better oxidation behaviour than the W-Cr-Y sample under given experimental conditions.

To clarify the oxidation product's changes with the oxidation time, Fig. 8a shows XRD spectra of the W-11.2Cr-1.7Zr as deposited, oxidation with 75 min and 10 h. Apart from the Cr_2O_3 and ZrO_2, which has been detected in W-Cr-Zr sample after oxidation of 75 min, two new oxides of Cr_2WO_6 (JCPDS # 73-2236) and WO_3 (JCPDS # 83-0949) could be detected in the oxide scale. Therefore, W element has been oxidized during the isothermal oxidation of 10 h. The corresponding cross section of the W-11.2Cr-1.7Zr sample was also characterized by SEM-FIB, as shown in Fig. 8b. Compared with Fig. 6c, the thickness of the formed oxide scale grows from ~ 310 nm to ~ 1 μm and the internal oxidation has obviously become worse because of the long-term oxidation. Notably, different from the dark oxide scale, two grey particles as denoted by black arrows exist at the top of the oxide scale. These two grey particles should be a newly formed oxide. To confirm the composition of the new oxide, a mapping spectrum was carried out in the indicated area as shown in Fig. 8b. The corresponding mapping images of W, Cr and O elements are also shown in Fig. 8b. From these mapping images, it can be concluded that the new oxide is composed of W, Cr and O. Combined with the XRD spectrum, it can be said that the new oxide corresponds to Cr_2WO_6 or the mixed oxides of WO_3 and Cr_2WO_6. Based on current understanding, the tungsten oxides were detected on the top surface of the protective mixed scale (Cr_2O_3 and ZrO_2), therefore, W oxidation in W-Cr-Zr system would be controlled by the W cations diffusing outwards from the thin film towards the oxidizing atmosphere.

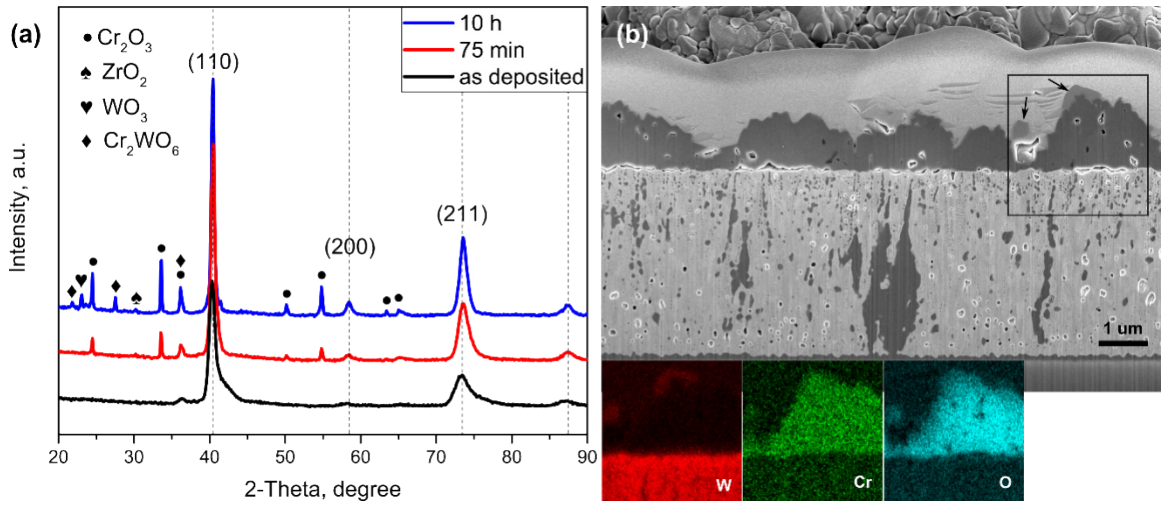

Fig. 8 (a) XRD spectra of W-11.2Cr-1.7Zr sample and (b) cross section of the W-11.2Cr-1.7Zr sample after isothermal oxidation for 10 h.

4. Discussion

4.1 Evaluation of composition optimization

In this work, the power law was used to describe the oxidation behaviour. The corresponding oxidation behaviour parameters (*K, n, T*) can directly reflect the oxidation behaviour. The oxidation behaviour of W-Cr-Zr sample correlates with its microstructure and composition. Although the W-Cr-Zr thin films have a homogeneous microstructure after magnetron sputtering, different composition will result in different oxide microstructure during the oxidation process. In the W-Cr-Zr system, variation of the Zr/Cr ratio in different Cr content can illustrate its composition changes. For a deeper study of the oxidation behaviour of W-Cr-Zr samples, establishment of a relationship between the oxidation behaviour parameters (*K, n, T*) and Zr/Cr ratio is shown in Fig. 9. The value of the Zr/Cr ratio of W-Cr-Zr samples is given in units of atomic percent. The oxidation behaviour parameters of oxidation coefficient, oxidation exponent and the passivating time are marked with red, blue and black symbols and lines, respectively. The solid lines denote the corresponding parameter with similar Cr content, and the dotted lines denote the corresponding parameter with similar Zr content. From Fig. 9, these oxidation behaviour parameters are closely related to the Zr/Cr ratio of the W-Cr-Zr sample. Under the premise of the similar Cr or Zr content, the oxidation coefficient decreases first and then increases as Zr/Cr ratio increases. Remarkable, that the oxidation exponent shows an opposite trend: it increased and then decreases as Zr/Cr ratio grows. Turning the attention to the passivating time, where presents a change trend that increases first and then decreases as Zr/Cr ratio increases. Remarkably, the passivating time has a great fluctuation in a range between ~5% and ~10% of Zr/Cr ratio, which indicates that there exists an optimal Zr/Cr ratio value that has a longest passivating time. This finding is beneficial for material composition design and find out a promising W-Cr-Zr self-passivating alloy with an optimal oxidation resistance.

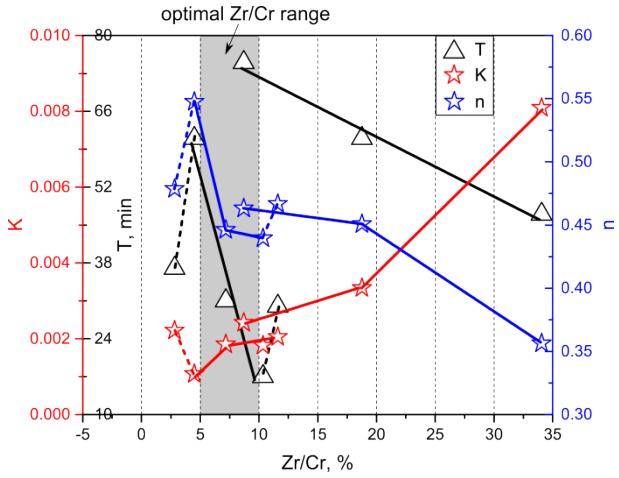

Fig. 9 The oxidation coefficient (K), oxidation exponent (n) and passivating time (T) of the W-Cr-Zr samples over Zr/Cr ratio change (atomic ratio). The different colours represent the different parameters. The solid lines show the corresponding parameter with similar Cr content, and the dotted lines mean the corresponding parameter with similar Zr content.

An excellent self-passivating W alloy must possess a long passivating time, which requires a high quality (dense) initial thin oxide scale to prevent W oxidation and a low growth rate of the oxide scale. In the W-Cr-Zr system, Cr as a passivating element is responsible to form the Cr_2O_3 oxide scale, while Zr acts as the active element to improve the oxidation behaviour. Zr has a higher oxygen affinity than the passivating element Cr [17]. Thus, the initial oxide scale must involve two oxides of ZrO_2 and Cr_2O_3, which can be deduced from XRD spectra in Fig. 5. The microstructure of the oxide scale is that the ZrO_2 particles are dispersed in the Cr_2O_3 scale matrix. Different composition of W-Cr-Zr system will result in different microstructure of the formed oxide scale during the oxidation. The quality of the initial oxide scale can be estimated by internal oxidation. Poor quality of the initial oxide scale will help oxygen getting through the oxide scale and results in internal oxidation. Therefore, deeper internal oxidation means a worse initial oxide scale. In Fig. 6, the W-12.5Cr-0.6Zr and W-12.1Cr-7.0Zr samples show deep internal oxidation, meaning that W-12.5Cr-0.6Zr and W-12.5Cr-7.0Zr samples have a poor quality initial oxide scale, which is due to either too low or too high Zr/Cr ratio. Too low Zr/Cr ratio means low Zr addition and low Zr influence, which is close to the W-Cr binary system. Hence, it is easy to understand that the W-12.5Cr-0.6Zr sample after oxidation of 75 min contains tungsten oxides ($CrWO_4$ and WO_3) and presents a deep internal oxidation. Generally, the role of active elements has indicated that the beneficial effects are more pronounced if the active element fraction does not exceed some low concentration, whereas higher active element concentrations will result in undesirable negative effects [13]. For the W-Cr-Zr thin film systems, the dispersive distribution of ZrO_2 fine particles can suppress the Cr_2O_3 scale growth at a low Zr active element concentration. Addition of further Zr increases the ZrO_2 particles size, which would decrease the adhesion between oxide scale and matrix. Therefore, too high Zr/Cr ratio can also result in a poor quality initial oxide scale. In this sense, the experimental studies do support the analytical considerations using the power law, on existence of an optimal Zr/Cr ratio value that has a longest passivating time for the W-Cr-Zr self-passviating alloy. Notably, the W-10.5Cr-1.3Zr and W-11.2Cr-1.7Zr samples have a similar Zr/Cr ratio but there exist an obvious difference in passivating time. The reason is due to the W-11.2Cr-1.7Zr sample possesses a higher and sufficient Cr content. It is implying that different Cr content may be the reason why the passivating time has an obvious fluctuation in the optimal range between 5% and 10% of Zr/Cr ratio. The W-11.2Cr-1.7Zr sample with a higher Cr content and an optimal Zr/Cr ratio possesses a high quality initial oxide scale, hence, its internal oxidation is located close to the surface. Therefore, from the material composition design perspective, a promising W-Cr-Zr self-passivating alloy requires sufficient Cr content and an optimum Zr/Cr ratio. These two samples have a similar oxidation exponent, but the W-11.2Cr-1.7Cr sample

presents a higher oxidation coefficient than the W-10.5Cr-1.3Zr sample. Therefore, the current dependencies between oxidation behaviour parameters and oxidation experiment would mean that the Zr/Cr ratio is directly related to the oxidation exponent, whereas the oxidation coefficient in turn is indicating whether there is enough of the passivating element Cr in the alloy as required to form a high quality initial oxide scale. This crucial microstructural feature of the initial oxide scale is responsible for the improvement of self-passivating behaviour, which is related to the distribution of the active element in the material during the oxidation. The oxidation coefficient of W-11.2Cr-1.7Zr sample locates at a moderate value (Fig. 9), implying that a dense initial thin oxide scale requires primarily a suitable oxidation coefficient. Furthermore, a lower oxidation exponent means a low growth rate of the oxide scale. Therefore, an excellent self-passivating W alloy with a long passivating time requires a suitable oxidation coefficient and a lower oxidation exponent.

4.2 Influence of Zr

In the W-Cr-Zr thin film system, Zr as the active element improves the oxidation behaviour. Therefore, it is necessary to study how Zr influences Cr behaviour during the oxidation process. Fig. 10 shows the oxidation curves of the pure Cr, Cr-Zr and Cr-Cr/Zr samples oxidized under identical conditions for 1 h at 1000 ºC, which are marked with different solid colour lines. According to the power law, the corresponding fitting curves are depicted by the red dotted lines. The oxidation curves directly reflect the oxidation process of the thin film samples. For the Cr-Zr and Cr-Cr/Zr samples, the oxidation curves at the initial few minutes reveal the oxidation behaviour of the Zr or Cr/Zr surface layer. Hence the corresponding fitting curves start a few minutes later, which reflect continuous Cr oxidation. The parameters of oxidation coefficient and oxidation exponent are also shown in Fig. 10. These three samples are showing self-passivating behaviour within the oxidation time. The pure Cr sample has the highest mass change after oxidation, while the Cr-Cr/Zr sample has the lowest mass change, which is almost half of the mass change of the Cr-Zr sample. This is owing to the fact, that the Cr-Cr/Zr sample has the lowest oxidation coefficient and the lowest oxidation exponent.

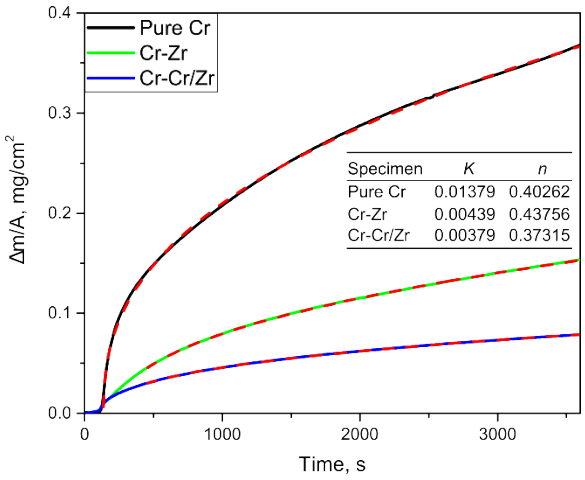

Fig. 10 The oxidation curves of pure Cr, Cr-Zr and Cr-Cr/Zr samples with an isothermal time of 1 h.

From the oxidation coefficient perspective, the pure Cr sample has the highest oxidation coefficient and presents a fast mass change at the initial few moments of exposure. The initially formed oxide scale correlates with an oxidation coefficient. For the Cr-Zr or Cr-Cr/Zr samples with double-layered structure, the surface Zr layer or Cr/Zr composite layer must be preferentially oxidized and form the corresponding oxide scale during the oxidation process. Thus, it is easy to understand that the Cr-Zr and Cr-Cr/Zr samples have a lower oxidation coefficient compared to that of the pure Cr sample. Comparing the pure Cr sample to the Cr-Cr/Zr sample, the Cr-Cr/Zr sample has an initial composite oxide scale that results in a lower oxidation coefficient. It indicates that the Zr active element additions can accelerate the formation

of the initial oxide scale simultaneously reducing the depletion of Cr. For the Cr/Zr composite layer on the top surface of the Cr-Cr/Zr sample, Zr element prefers to oxidize and then act as the nucleation sites to accelerate oxide nucleation and formation of the initial oxide scale.

When we look ongoing process from the oxidation exponent perspective, the oxidation exponent of the Cr-Zr sample is slightly higher than that of pure Cr sample. At the high temperature of 1000 °C, the formed oxides would be ionization. During the ionization process, the oxygen concentration of the ZrO_2 scale on the surface of the Cr-Zr sample would be higher than that of pure Cr with a Cr_2O_3 scale on the surface. High oxygen concentration is beneficial for Cr depletion, which reflects in a high oxidation exponent. Furthermore, the Cr-Cr/Zr sample has a lower oxidation exponent as compared to the pure Cr sample. The oxidation exponent is closely related to the continuous growth rate of the oxide scale. Notably, the mechanism of Cr oxidation is controlled by Cr cation diffusion outward [27]. This means that Zr as an active element can reduce the oxidation rate and Cr depletion by hindering Cr cation diffusion. Based on the abovementioned analysis, Zr additions have an effect not only on the oxidation coefficient but also affect the oxidation exponent.

XRD was also used to characterize the Cr-Zr and Cr-Cr/Zr samples before and after the oxidation, the corresponding XRD spectra are shown in Fig. 11. The Cr-Zr and Cr-Cr/Zr samples as deposited are composed of Cr (JCPDS # 06-0694) and Zr (JCPDS # 88-2329) phase. For the Cr-Zr sample after oxidation of 1 h, the oxide scale contains Cr_2O_3 and two kinds of ZrO_2 oxides (JCPDS # 86-1449 and JCPDS # 49-1642). For the Cr-Cr/Zr sample, the formed oxide scale is also composed of Cr_2O_3, but only one kind of ZrO_2 (JCPDS # 49-1642). Comparing the XRD spectra between these double-layered samples (Fig. 11) and W-Cr-Zr system (Fig. 5), the formed initial oxide scales are mainly composed by Cr_2O_3 and ZrO_2. Therefore, Zr influence in double-layered samples would be similar to the case of the W-Cr-Zr system.

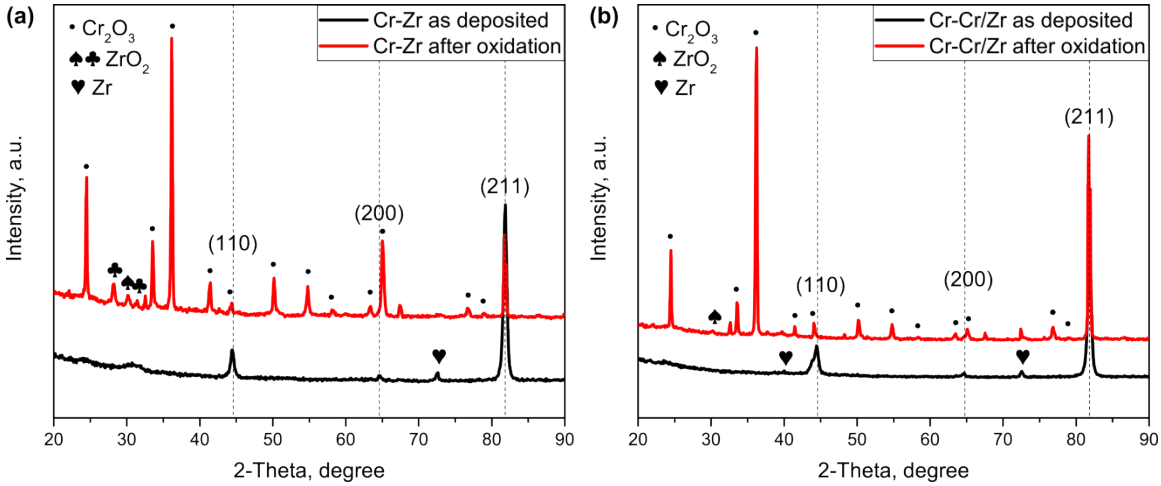

Fig. 11 The XRD spectra of Cr-Zr and Cr-Cr/Zr samples as deposited and after oxidation test.

The cross section of the Cr-Zr and Cr-Cr/Zr samples is also characterized by SEM-FIB and the corresponding images are shown in Fig. 12. In addition, the depth profiles of Cr and Zr are also presented in Fig. 12. These are obtained from the SIMS measurement. Figs. 12a and 12b show the Cr-Zr and Cr-Cr/Zr samples as deposited, respectively. From the corresponding SIMS results, the surface layers are the Zr layer and the Cr/Zr composite layer, respectively, which agree with what we designed. For the oxidation process of the Cr-Zr sample, the Zr layer would be first oxidized on the top surface, subsequently, the sub-surface layer of Cr layer would begin to oxidize. The cross section and the SIMS profiles are presented in Fig. 12c. The Zr depth profile shows that the Zr cation only exists on the surface, whereas the Cr depth profile shows that the Cr cation mainly exists in the sub-surface. Combined with the XRD spectra in Fig. 11a, the surface oxide layer is ZrO_2 and the oxide in the sub-surface is Cr_2O_3. The

oxidation of metals or alloys at high temperature can be depicted as ion diffusion process [19-22]. For the oxidation of the Cr-Zr sample, the Cr_2O_3 scale grows by outward diffusion of Cr cation. The Cr cation diffusion would result in vacancy accumulation and the formation of voids beneath the Cr_2O_3 scale [27] as shown in Fig. 12c. Notably, there is no Cr_2O_3 detected on the top of the surface of the ZrO_2 layer, which implies that the Cr cation diffusion through ZrO_2 scale was required to overcome a higher energy barrier than O anion through ZrO_2 scale. From the phase diagram [29], the solubility of Cr in ZrO_2 is very low at 1000 °C, indicating that the Cr cation is hard to diffuse through the ZrO_2 layer. Therefore, the ZrO_2 can reduce the Cr element oxidation by hindering Cr cation diffusion.

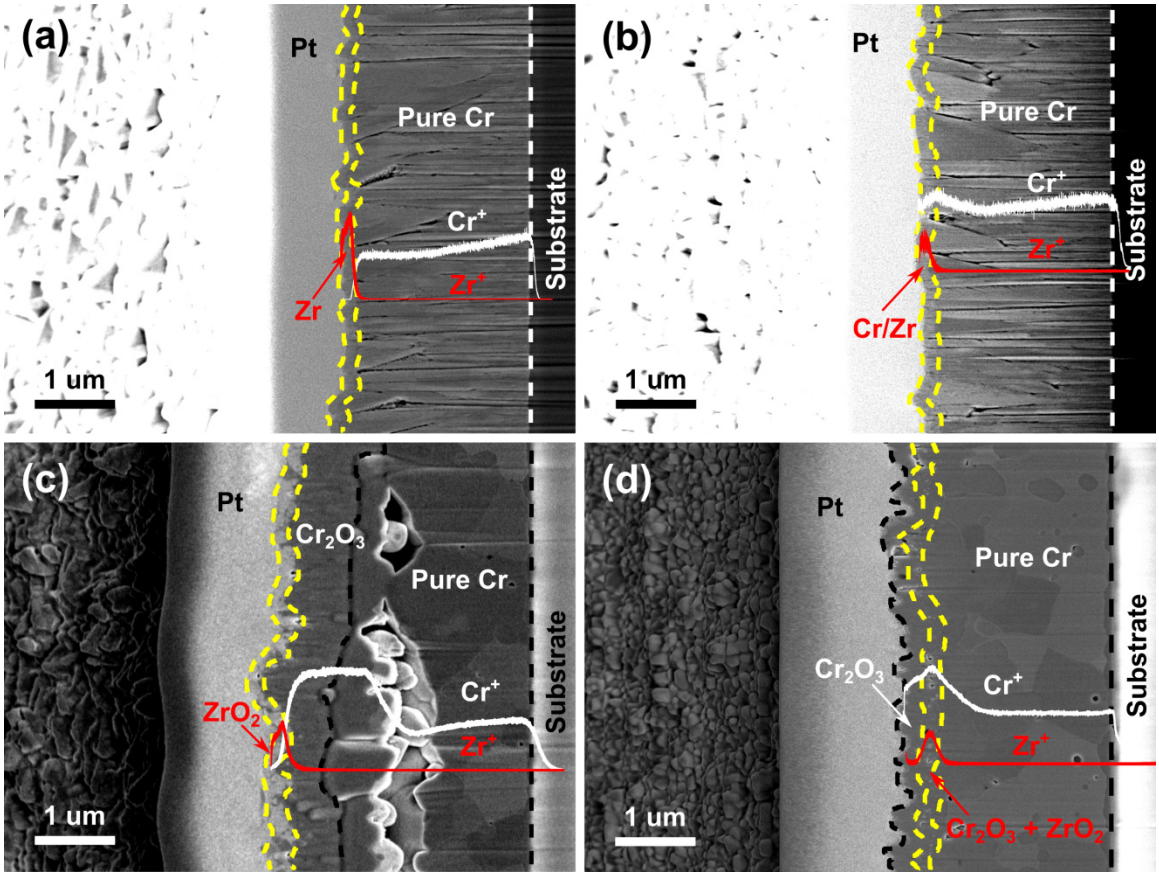

Fig. 12The cross-section of (a) Cr-Zr sample as deposited, (b) Cr-Cr/Zr sample as deposited, (c) Cr-Zr sample after oxidation test (d)Cr-Cr/Zr sample after oxidation test. In (a) - (d), the corresponding SIMS profiles were marked on SEM images.

For the Cr-Cr/Zr sample, the Cr/Zr composite layer would be preferentially oxidized and form a composite oxide scale already in the beginning of the oxidation process. In the course of oxidation, the sub-surface layer of Cr layer begins to oxidize and forms a new oxide scale. From the SIMS depth profiles in Fig. 12d, the Zr cation exists in the sub-surface, whereas the Cr cation is distributed on the surface and sub-surface i.e. Cr/Zr layer is not blocking Cr diffusion outwards as mentioned in previous case. Combined with the XRD spectra in Fig. 11b, the composite oxide scale composed of Cr_2O_3 and ZrO_2 is located at the sub-surface. Notably, the new oxide scale is Cr_2O_3 and formed on the top of the composite oxide scale, which should be due to the Cr cation could diffuse through the composite oxide scale. Unfortunately, these layers of the new Cr_2O_3 scale, composite oxide scale and the pure Cr layer are hard to be distinguished because of their low contrast difference. For better understanding the thin film structure after oxidation, these almost invisible interfaces are also marked with yellow dotted lines. The low visibility of the interfaces is believed to be due to some micro-pores as visible e.g. in Fig. 12d.

Compared to the Cr-Zr sample, there is no big pore structure beneath the oxide scale, which may originate from the Zr active element reducing Cr diffusion. In addition, the thickness of the oxide layer for the Cr-Cr/Zr sample is almost half of the thickness of the oxide layer for the Cr-Zr sample, which agrees well with the mass changes of the responding samples in Fig. 10.

Generally, Fig. 12c indicates ZrO_2 as the diffusion barrier can hinder Cr cation diffusion during the oxidation process. For the Cr-Cr/Zr sample after the initial few moments of oxidation, the composite oxide scale possesses a microstructure with dispersed ZrO_2 particles which can distribute in the Cr_2O_3 matrix. Thus, these ZrO_2 particles can decrease the Cr cation diffusion and then reduce Cr depletion. This would be the reason why the Cr-Cr/Zr sample has a lower oxidation exponent compared to the pure Cr. Therefore, as mentioned above, due to higher O-affinity of Zr, Zr oxidizes preferentially and acts as the nucleation sites for Cr oxidation and subsequently leads to formation of the initial composite oxide (Cr_2O_3 and ZrO_2) scale. In the progress of oxidation, the formed ZrO_2 particles can reduce Cr depletion, that is, decrease the oxidation rate, and thus prolong the passivating time. This is the reason why W-Cr-Zr system has no significant inflection point from the self-passivating to the linear stage. Therefore, Zr as an active element can play the decisive role to improve the high temperature oxidation behaviour of W-Cr-Zr thin film system.

5. Conclusions

In this work, a power law was used to evaluate the oxidation curves of W-Cr-Zr thin film alloys. As the analysis shows, an excellent self-passivating W alloy must possess a long passivating-time and thus requires a suitable oxidation coefficient and a lower oxidation exponent. A suitable oxidation coefficient is beneficial to form a dense initial thin oxide scale whereas a lower oxidation exponent means a low growth rate of the oxide scale during the further progression.

To find an optimum the composition of the W-Cr-Zr system, the relationship between the oxidation parameters (*K, n, T*) and the Zr/Cr ratio was investigated. Our analyses led to the conclusion, the oxidation coefficient decreases first and then increases as Zr/Cr ratio rises, whereas the oxidation exponent shows the opposite behaviour to the oxidation coefficient. The longest passivating time was attained for an optimum Zr/Cr ratio in the range between ~5% and ~10%.

According to the power law fitting function, the pure W sample has an oxidation component of ~1.56, which is larger than 1, indicating that the pure W oxidation behaviour is worse than linear oxidation behaviour. For the ternary alloys at a ten-hour oxidation, the oxidation process contains a self-passivating stage followed by a linear stage. The W-Cr-Y sample has a significant inflection point from the self-passivating stage to the linear stage, while the W-Cr-Zr samples have a smooth transition between those two stages. This indicates that W-Cr-Zr thin film system show better oxidation behaviour than the W-Cr-Y thin film system under given experimental conditions. Remarkably, the W-11.2Cr-1.7Zr sample with a thickness of ~4 μm possesses a passivating time of ~3 h.

Based on the experiments related to the influence of the Zr, additions of Zr not only have an effect on the oxidation coefficient but also affect the oxidation exponent. Zr as an active element during the oxidation is prone to forming nucleation sites in order to assist an initial oxide scale and then reduce oxidation by hindering Cr cations diffusion. Therefore, Zr as active element plays the key role in improvement the high temperature oxidation behaviour of the W-Cr-Zr thin film system.

For the W-Cr-Zr ternary alloy, the Cr passivating element aims at forming the protective oxide scale, while the Zr active element acts on improving the oxidation resistance. In the case of long-term oxidation, the Cr depletion will result in W oxidation. Therefore, detailed studies of the influence of the formed oxide scale on the W oxidation are essential. In addition, preparation of the W-Cr-Zr ternary bulk alloy and observation of the corresponding oxidation behaviour are necessary for future investigations.

Acknowledgments

This work has been carried out within the framework of the EUROfusion Consortium and has received funding from the Euratom research and training programme 2014-2018 under grant agreement No 633053. The views and opinions expressed herein do not necessarily reflect those of the European Commission. Authors acknowledge funding support from China Scholarship Council, National Magnetic Confinement Fusion Program (Grant No. 2014GB121001 and 2014GB121001B), National Natural Science Foundation of China (Grant No. 51574101, 51474083, 51674095, and 51675154) and the 111 project "New Materials and Technology for Clean Energy" (Grant No. B18018).

References

[1] X.Y. Tan, L.M. Luo, H.Y. Chen, X.Y. Zhu, X. Zan, G.N. Luo, J.L. Chen, P. Li, J.G. Cheng, D.P. Liu, Y.C. Wu. Mechanical properties and microstructural change of W-Y_2O_3 alloy under helium irradiation. Sci. Rep. 5 (2015) 12755.
[2] D. Maisonnier, I. Cook, S. Pierre, B. Lorenzo, D.P. Luigi, G. Luciano, N. Prachai, P. Aldo, PPCS Team. DEMO and fusion power plant conceptual studies in Europe. Fusion Eng. Des. 81 (2006) 1123-1130.
[3] T. Wegener, F. Klein, A. Litnovsky, M. Rasinski, J. Brinkmann, F. Koch, Ch. Linsmeier. Development of yttrium-containing self-passivating tungsten alloys for future fusion power plants. Nucl. Mater. Energy 9 (2016) 394-398.
[4] A. Litnovsky, T. Wegener, F. Klein, Ch. Linsmeier, M. Rasinski, A. Kreter, B. Unterberg, J.W. Coenen, H. Du, J. Mayer, C. Garcia-Rosales, A. Calvo and N. Ordas. Smart tungsten alloys as a material for the first wall of a future fusion power plant. Nucl. Fusion 57 (2017) 066020.
[5] F. Koch, S. K□ppl, H. Bolt. Self passivating W-based alloys as plasma-facing material. J. Nucl. Mater. 386-388 (2009) 572-574.
[6] P. López-Ruiz, N. Ordás, S. Lindig, F. Koch, I. Iturriza and C. García-Rosales. Self-passivating bulk tungsten-based alloys manufactured by powder metallurgy. Phys. Scr. T145 (2011) 014018.
[7] A. Litnovsky, T. Wegener, F. Klein, Ch. Linsmeier, M. Rasinski, A. Kreter, X. Tan, J. Schmitz, Y. Mao, J.W. Coenen, M. Bram and J. Gonzalez-Julian. Advanced smart tungsten alloys for a future fusion power plant. Plasma Phys. Control. Fusion 59 (2017) 064003.
[8] N.B. Pilling, R.E. Bedworth. The oxidation of metals at high temperatures. J. Inst. Met. 29 (1923), S. 529-591.
[9] D.J. Young, J. Zurek, L. Singheiser, W.J. Quadakkers. Temperature dependence of oxide scale formation on high-Cr ferritic steels in Ar-H2-H2O. Corros. Sci. 53 (2011) 2131-2141.
[10] H. Wang, W. Yan, S. van Zwaag, Q. Shi, W. Wang, K. Yang, Y. Shan. On the 650 ºC thermostability of 9-12Cr heat resistant steels containing different precipitates. Acta Mater. 134 (2017) 143-154.
[11] M.-Y. Kim, S.-M. Hong, K.-H. Lee, W.-S. Jung, Y.-S. Lee, Y.-K. Lee, J.-H. Shim. Mechanism for Z-phase formation in 11CrMoVNbN martensitic heat-resistant steel. Mater. Charact. 129 (2017) 40-45.
[12] T. Wegener, F. Klein, A. Litnovsky, M. Rasinski, J. Brinkmann, F. Koch, Ch. Linsmeier. Development and analyses of self-passivating tungsten alloys for DEMO accidental conditions. Fusion Eng, Des. (2017), http://dx.doi.org/10.1016/j.fusengdes.2017.03.072
[13] E. Lang. The role of active elements in the oxidation behaviour of high temperature metals and alloys. Commission of the European Communities, ISBN 1-85166-420-3.
[14] M.F. Pillis, O.V. Correa, E.G. de Araújo, L.V. Ramanathan. Oxidation Behaviour of FeCr and FeCrY Alloys Coated with an Aluminium Based Paint. Mat. Res. 11(2008)3: 251-256.
[15] E.J. Felten. High-Temperature Oxidation of Fe-Cr Base Alloys with Particular Reference to Fe-Cr-Y Alloys. J.Electrochem. Soc.408 (1961) 6: 490-495.
[16] A. Calvo, C. García-Rosales, N. Ordás, I. Iturriza, K. Schlueter, F. Koch, G. Pintsuk, E. Tejado, J.Y. Pastor. Self-passivating W-Cr-Y alloys: Characterization and testing. Fusion Eng. Des. (2017), http://dx.doi.org/10.1016/j.fusengdes.2017.03.001
[17] I. Barin. Thermochemical Data of Pure Substances. Third edition 1995 Weinheim:VCH.

[18] M.R. Gilbert, J.-Ch.Sublet. Handbook of activation, transmutation, and radiation damage properties of the elements simulated using FISPACT-II & TENDL-2015; Magnetic Fusion Plants September 2016.
[19] S. Samal. High temperature corrosion. INTECH, Chapter 6 High-temperature oxidation of metals 101-121. http://dx.doi.org/10.5772/6300.
[20] N. Cabrera, N.F. Mott. Theory of the oxidation of metal. Rep. Prog. Phys. 12(1949) 163-184.
[21] C. Wagner. Theoretical analysis of the diffusion processes determining the oxidation rate of alloys. J. Electrochem.Soc. October 1952, 369-380.
[22] G.C. Wood. High-temperature oxidation of alloys. Oxid. of Met.2 (1970) 1: 11-57.
[23] D. Yong. High temperature oxidation and corrosion of metals. First edition, Elsevier Science 6th August 2008. ISBN:9780080559414
[24] G. Tammann, Z. Anorg. Über Anlauffarben von Metallen. Allg. Chem., 111(1920)78-89.
[25] A.T. Fromhold. Theory of metal oxidation. North Holland Publishing Company, Amsterdam (1976). Signatur an der Bibliothek der Uni Graz:I 466591.
[26] F. Morin, G. Beranger, and P. Lacombe. Limits of application for Wagner's oxidation theory. Oxid. Met. 4 (1972) 1: 51-61.
[27] D. Caplan and G.I. Sproule. Effect of oxide grain structure on the high-temperature oxidation of Cr. Oxid. Met. 9 (1975) 5: 459-472.
[28] T. Onishi, S. Nakakubo and M. Takeda. Calculations of internal oxidation rate equations and boundary conditions between internal and external oxidation in silicon containing steels. Mater. Trans. 51 (2010) 3: 482-487.
[29] http://materials.springer.com/isp/phase-diagram/docs/c_0207809